RSC Advances

PAPER

View Article Online
View Journal | View Issue



Cite this: *RSC Adv.*, 2022, **12**, 6054

# Dynamic experiment on the treatment of acidic chromium-containing wastewater by lignite loaded nano FeS†

Xuying Guo, *[ab] Xinle Gao,[a] Saiou Fu,[c] Guoliang Jiang,[c] Yanrong Dong[c] and Zhiyong Hu [a]

In terms of the problem of severe pollution to the ecological environment caused by the acidic chrome-containing wastewater produced in the tanning, electroplating, metallurgy, printing and dyeing and other industries, based on the good adsorbability, reducibility and other properties of heavy metals such as Cr(VI) by lignite and nano FeS, the lignite-loaded nano FeS adsorbing material (nFeS-lignite) was prepared by ultrasonic precipitation method. NFeS-lignite and lignite were used as fillers to construct 1# and 2# dynamic columns to carry out the dynamic treatment experiment of acidic chrome-containing wastewater. And nFeS-lignite and lignite were characterized by XRD, SEM and EDS to explore the regularity, long-acting properties and removal mechanism of acidic chrome-containing wastewater treated by NFeS-lignite and lignite. The results indicate that: ① during 25 days of operation, the average removal percentages of Cr(VI) in the 1# and 2# dynamic columns are 71.6% and 53.1%. The average removal percentages of total chromium in 1# and 2# dynamic columns are 54.4% and 28.8%, and the average effluent pH of 1# and 2# dynamic columns is 5.3 and 7.3. ② According to XRD, SEM, EDS and FTIR analysis, the reducing groups in the structure of nFeS-lignite, such as $-CH_3$, $-CH_2$, C–O and Ar-OH, participate in the reaction and are oxidized to C=C, C=O and other groups. A large number of sediment crystals appeared on the particle surface, and new diffraction peaks such as FeOOH, $Cr(OH)_3$ and $Cr_2S_3$ appeared at the same time, indicating that after Cr(VI) was reduced to Cr(III), it would be fixed on the surface of nFeS-lignite in the form of precipitation such as hydroxide and sulfide.

Received 7th December 2021
Accepted 14th February 2022

DOI: 10.1039/d1ra08892k

rsc.li/rsc-advances



## 1 Introduction

Due to its unique physical and chemical properties, chromium is widely used in tanning, electroplating, metallurgy, printing and dyeing,[1] and the wastewater and waste residue discharged from industrial production become the main source of acid chromium containing wastewater.[2] Chromium mainly exists in two valence states of Cr(VI) and Cr(III),[3] in which the toxicity of Cr(VI) is hundreds of times higher than that of Cr(III).[4,5] Direct emission will cause serious harm to the environment and threaten human health through gradual accumulation in the food chain.[6] At present, common treatment technologies for acid chromium containing wastewater include chemical precipitation,[7] biological method,[8] ion exchange method,[9] adsorption method,[10] *etc.* The adsorption method has the advantages of low cost, simple operation and wide application, so it has a good application prospect.[11] Nazir *et al.*[12,13] prepared porous composite materials for adsorption studies on malachite green (MG) and methyl orange (MO) in water for many times. The results show that the porous composite has good adsorption effect on MG and MO, and its adsorption capacity is better than other single-phase materials. Khan *et al.*[14] synthesized graphene oxide and MOF based composite material and explored its adsorption effect on antibiotics. The results showed that the adsorption capacity of norfloxacin on the composite was 1114.82 mg $g^{-1}$, and the removal rate was more than 93%.

Nano FeS has good adsorption and reducibility, is environmentally friendly, cheap and easy to obtain, and has a good effect on removing Cr(VI) and other heavy metal pollutants. Liu *et al.*[15] prepared nano FeS by homogeneous precipitation method. Through orthogonal test, the preparation conditions such as $Na_2S$ solution concentration, stirring speed, stabilizer dosage and $Na_2S$ solution drop acceleration were optimized. The unit removal of Cr(VI) by nano FeS prepared under the optimal conditions was as high as 683 mg $g^{-1}$. After 15 minutes of reaction, the Cr(VI) removal rate could reach 92.48%. Yang *et al.*[16] treated acidic cadmium containing wastewater with the

[a]*College of Mining, Liaoning Technical University, Fuxin 123000, Liaoning, China. E-mail: guoxuying@lntu.edu.cn*

[b]*College of Science, Liaoning Technical University, Fuxin 123000, Liaoning, China*

[c]*College of Civil Engineering, Liaoning Technical University, Fuxin 123000, Liaoning, China*

† Electronic supplementary information (ESI) available. See DOI: 10.1039/d1ra08892k

prepared biological nano FeS. The research shows that increasing the reaction temperature can promote the removal of $Cd^{2+}$ by biological nano FeS. At 25 °C, 99.93% of $Cd^{2+}$ can be removed by reacting biological nano FeS with acidic cadmium containing wastewater for 15 minutes. However, nano FeS is easy to settle, oxidize and agglomerate in the preparation and test process. Therefore, it is necessary to choose a cheap and easy to obtain adsorption material with large specific surface area as the carrier.

Lignite reserves account for about 13% of China's total coal reserves.[17] It has the characteristics of developed pore structure and high specific surface area. These characteristics make lignite have good adsorption, complexation and ion exchange capacity for heavy metals and other pollutants. Therefore, it is often used as an efficient and low-cost adsorption material in environmental treatment. Jellali *et al.*[18] studied the removal capacity of lignite for $Cd^{2+}$ and $Cu^{2+}$ in water. The results show that the saturated adsorption capacity of lignite for $Cd^{2+}$ and $Cu^{2+}$ can reach 38.0 mg $g^{-1}$ and 21.4 mg $g^{-1}$. The removal rate of $Cd^{2+}$ is particularly rapid. 78% of $Cd^{2+}$ can be removed in one minute. Di *et al.*[19] used lignite/maifan stone combined with SRB to prepare immobilized particles to treat chromium containing acid mine wastewater. The results show that the treatment effect of lignite immobilized SRB particles on chromium containing acid wastewater is better than maifan stone immobilized SRB particles, and the removal rates of $Cr^{6+}$ and $SO_4^{2-}$ are 96.57% and 36.50% respectively. However, lignite has the characteristics of low removal per unit and slow removal efficiency, so loading modification of lignite with nano-materials with fast reaction rate becomes the focus of research.

Based on this, this study uses lignite as the supporting material and uses ultrasonic precipitation method to prepare lignite supported nano FeS new composite adsorption material (nFeS-lignite). NFeS-lignite can not only solve the agglomeration phenomenon of FeS in production and use, make full use of the advantages of large specific surface area of FeS, so that it can quickly react with Cr(VI), but also solve the shortcomings of low removal amount per lignite unit. Ensure that lignite and FeS play a maximum role in the treatment of acidic chromium-containing wastewater. The dynamic effects and pH changes of Cr(VI) and total chromium in acidic chromium containing wastewater treated by nFeS-lignite and lignite were studied. By constructing nFeS-lignite and lignite particle dynamic columns, the long-term treatment capacity of nFeS-lignite for acid chromium containing wastewater was explored. Combined with XRD, SEM EDS and FTIR analysis, the mechanism of lignite loaded nano FeS in the treatment of acid chromium containing wastewater is revealed, which provides a new idea for the treatment of acid chromium containing wastewater.

# 2 Materials and methods

## 2.1 Experimental materials

Lignite: selected from Dabeigou coal mine, Datong City, Shanxi Province. The main chemical composition is shown in Table 1. The lignite is crushed and screened. According to the preliminary test, lignite with particle size of 0.18–0.25 mm (60–80 mesh) is selected to prepare lignite loaded nano FeS.[20] The main components of lignite are shown in Table 1.

Acidic chromium-containing wastewater: laboratory simulation of acidic chromium-containing wastewater, using $K_2Cr_2O_7$ equipped with Cr(VI) concentration of 100 mg $L^{-1}$, pH = 4 acidic chromium-containing wastewater.

## 2.2 Experimental method

**2.2.1 Preparation method of lignite loaded nano FeS.** Lignite supported nano FeS (nFeS-lignite) adsorption materials were prepared by ultrasonic precipitation method, and some experimental parameters were formulated in combination with preliminary experimental studies.[6] Specific operations are as follows:

(1) 4 g of lignite was added to 200 mL of $Na_2S$ solution with a certain concentration, and stirred by magnetic stirrer for 8 h. At this point, the absorption of $S^{2-}$ by lignite reaches saturation. Stand for 3–5 min to make lignite particles settle at the bottom of the conical bottle. Slowly pour off the $Na_2S$ solution, leaving only the lignite particles at the bottom of the conical flask.

(2) Place the conical bottle containing lignite particles in the ultrasonic cleaning machine. 200 mL $FeSO_4$ solution was prepared according to a certain FeS molar ratio. TDrops of $FeSO_4$ solution were added to conical bottles at room temperature with a peristaltic pump at a flow rate of 0.44 mL $s^{-1}$. Stirring was carried out with a mechanical agitator at a speed of 350 rpm and ultrasonic treatment was performed at a frequency of 40 kHz for 10 min.

(3) After the ultrasonic treatment, the suspension was centrifuged at 4000 rpm for 15 min. Wash it three times with deionized water. The samples were refrigerated at 4 °C and sealed for later use.

**2.2.2 Construction of dynamic test device and experimental method.** Two plexiglass tubes with inner diameter of 40 mm and height of 200 mm are used. The test device system is shown in Fig. 1. The 1# column is filled with nFeS-lignite prepared under the conditions of lignite particle size of 0.18–0.25 mm, $Na_2S$ concentration of 0.30 mol $L^{-1}$ and iron sulfur molar ratio of 2.5 : 1, and the 2# column is filled with lignite particle size of 0.18–0.25 mm with a filling height of 100 mm. The peristaltic pump is used to pass the acid chromium containing wastewater into the dynamic column in the form of "bottom-up". In order to ensure the stability of inlet water flow and avoid material loss, 40 mm glass beads are filled

Table 1 Main compositions of lignite

| Constituent | CaO | $SiO_2$ | $SO_3$ | $Fe_2O_3$ | MgO | $Al_2O_3$ | $TiO_2$ | SrO | CdO | $P_2O_5$ | MnO |
|---|---|---|---|---|---|---|---|---|---|---|---|
| Mass fraction/% | 40.39 | 22.26 | 11.98 | 9.74 | 6.46 | 6.11 | 0.90 | 0.88 | 0.53 | 0.39 | 0.36 |

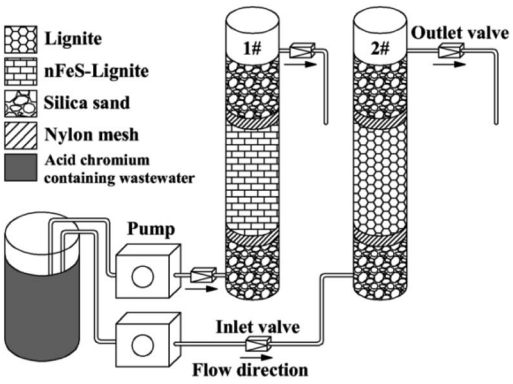


Fig. 1 Dynamic experiment device system.

at the upper and lower ends of the column, and a layer of nylon filter membrane is placed. The glass beads have been pickled and alkali washed with hydrochloric acid solution and sodium hydroxide solution in advance, and washed with deionized water to remove impurities and metal oxides on the surface of the glass beads. After the dynamic column is installed, deionized water is introduced into the column at a low flow rate to discharge the air in the column, so as to make the column reach stable saturation and avoid dominant flow. The hydraulic retention time of the dynamic column is 2.5 h and the pore velocity is 4 cm $h^{-1}$. Darcy velocity of each column was calculated according to the porosity of the dynamic column, and then the corresponding inlet flow of the peristaltic pump was determined. The specific test parameters of the dynamic column are shown in Table 2. Collect water samples every 8 h, determine pH value and residual concentrations of Cr(VI) and total chromium, and calculate their removal rate $\eta$.

$$\eta = \frac{C_0 - C_t}{C_0} \times 100\% \quad (1)$$

where: $\eta$ is the removal percentage, %; $C_0$ is the initial concentration, mg $L^{-1}$; $C_t$ is the residual concentration, mg $L^{-1}$.

**2.2.3 Water quality detection and material characterization methods.** Cr(VI) was determined by diphenylcarbazide spectrophotometry (China National Standard GB/T7467-87), total chromium was determined by potassium permanganate oxidation diphenylcarbazide spectrophotometry (China National Standard GB/T7466-87), and pH was determined by glass electrode method (China National Standard GB/T6920-86).

The micro morphology of acid chromium containing wastewater treated by lignite and nFeS-lignite was analyzed by Sigma 500 scanning electron microscope (SEM); the mineralogical composition of lignite and nFeS-lignite before and after the treatment of acid chromium containing wastewater was studied by Smart Lab 9X-ray (XRD).

# 3 Results and analysis

## 3.1 X-ray diffraction analysis

The X-ray diffraction pattern of lignite and nFeS-lignite before and after reaction is shown in Fig. 2.

It can be seen from Fig. 2a that the characteristic peak intensities of kaolinite and quartz after lignite reaction are weakened compared with those before reaction, and the peak intensities at $2\theta$ a new diffraction peak appears at the angle of 50.1°, which corresponds to the crystal plane diffraction of quartz (Minerals no .46-1045). This is because the lignite has been washed by acidic wastewater for a long time, the mineral components contained are gradually eroded by wastewater, and its structural properties change. The strength of the characteristic peak of minerals decreases with it, the acid resistance of quartz is strong, and new characteristic peaks are easy to appear after reaction. In addition, lignite reacted in $2\theta$ new diffraction peaks appear at angles of 27.6° and 41.4°, corresponding to the crystal plane diffraction of $Cr_2O_3$ (ICSD Patterns No. 25-1437), indicating that after lignite reduces Cr(VI) to Cr(III), Cr(III) is fixed on its surface by the reaction of oxygen-containing functional groups with Cr(III) to form $Cr_2O_3$ precipitation. It can be seen from Fig. 2b that after the nFeS-lignite reaction, the characteristic peak intensity of kaolinite and quartz further weakened, the characteristic peak of kaolinite could not be distinguished, and the FeS characteristic peak disappeared at $2\theta$ diffraction peaks appear at angles of 14.1°, 27.1° and 46.9°, corresponding to the crystal plane diffraction of FeOOH (ICSD Patterns no. 08-0098), at $2\theta$ new diffraction peaks appear at angles of 29.7°, 34.2° and 53.4°, corresponding to the crystal plane diffraction of $Cr_2S_3$ (ICSD Patterns no. 11-0007) $2\theta$ a new diffraction peak appears at the angle of 36.9°, corresponding to the crystal plane diffraction of $Cr(OH)_3$ (ICSD Patterns no. 20-0312), indicating that the loaded nano FeS completely reacts with Cr(VI) in the dynamic test, and most of the generated $Fe^{3+}$ is attached to the nFeS-lignite surface in the form of FeOOH precipitation, $S^{2-}$ is combined with Cr(III) to form $Cr_2S_3$ precipitation, and some Cr(III) will form $Cr(OH)_3$ precipitation with the increase of solution pH.

## 3.2 SEM analysis

Fig. 3 is a SEM diagram of lignite before and after reaction with nFeS-lignite. Comparing Fig. 3a and b, it can be seen that after lignite reaction, the surface gullies increase, the erosion phenomenon is obvious, the mineral structure is damaged,

Table 2 Parameters of the dynamic column

| Packing | The packing quality/(g) | Proportion | Void ratio | Darcy velocity/(cm $h^{-1}$) | Peristaltic pump flow rate/(mL $min^{-1}$) |
|---|---|---|---|---|---|
| nFeS-lignite | 107.93 | 1.4 | 0.39 | 1.55 | 0.32 |
| Lignite | 102.36 | 1.2 | 0.32 | 1.28 | 0.27 |

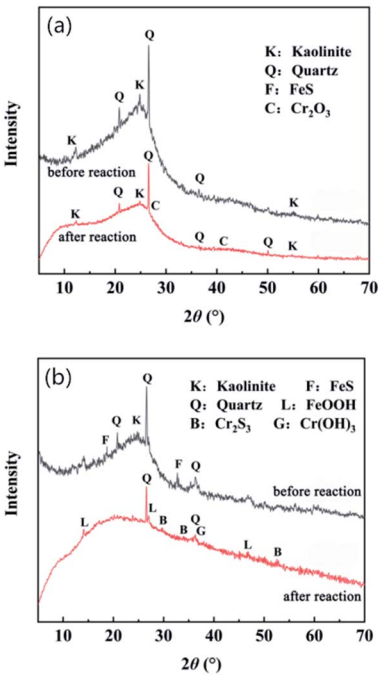


Fig. 2 XRD diffraction of lignite before and after the reaction with nFeS-lignite. (a) Lignite. (b) nFeS-lignite.

and a large number of irregular lines and fine sediments appear. Combined with the XRD analysis results, it can be seen that the sediment crystal may be $Cr_2O_3$ precipitation attached to the lignite surface. Comparing Fig. 3c and d, it can be seen that a large number of well dispersed nano FeS crystals are loaded on the surface of nFeS-lignite before the reaction, but after the reaction, the nano FeS crystals loaded by nFeS-lignite disappear, the surface of lignite particles as a carrier collapses, forming many micro pores, and spherical agglomerated crystals appear on the surface and pores of nFeS-lignite particles, combined with the XRD analysis results, the spherical agglomerated crystals should be FeOOH, $Cr_2S_3$ and $Cr(OH)_3$ precipitates formed after the reaction of nano FeS with Cr(VI) and Cr(III).

### 3.3 X-ray energy chromatography

Table 3 and Fig. 4 show the element content and X-ray energy chromatogram (EDS) before and after the reaction of lignite with nFeS-lignite.

Compared with lignite, the mass percentage of S element in nFeS-lignite increased from 2.58% to 17.80%, and the mass percentage of iron element increased from 1.34% to 37.66%, indicating that nano FeS was successfully loaded on the surface of lignite. Compared with that before the reaction, chromium appeared after the reaction of lignite and nFeS-lignite, and the mass percentages were 1.01% and 4.52% respectively, which proved that lignite and nFeS-lignite had a certain fixation ability for chromium. After the nFeS-lignite reaction, the mass percentage of sulfur decreases slightly, and the proportion of iron changes little. It is confirmed that part of $S^{2-}$ will combine

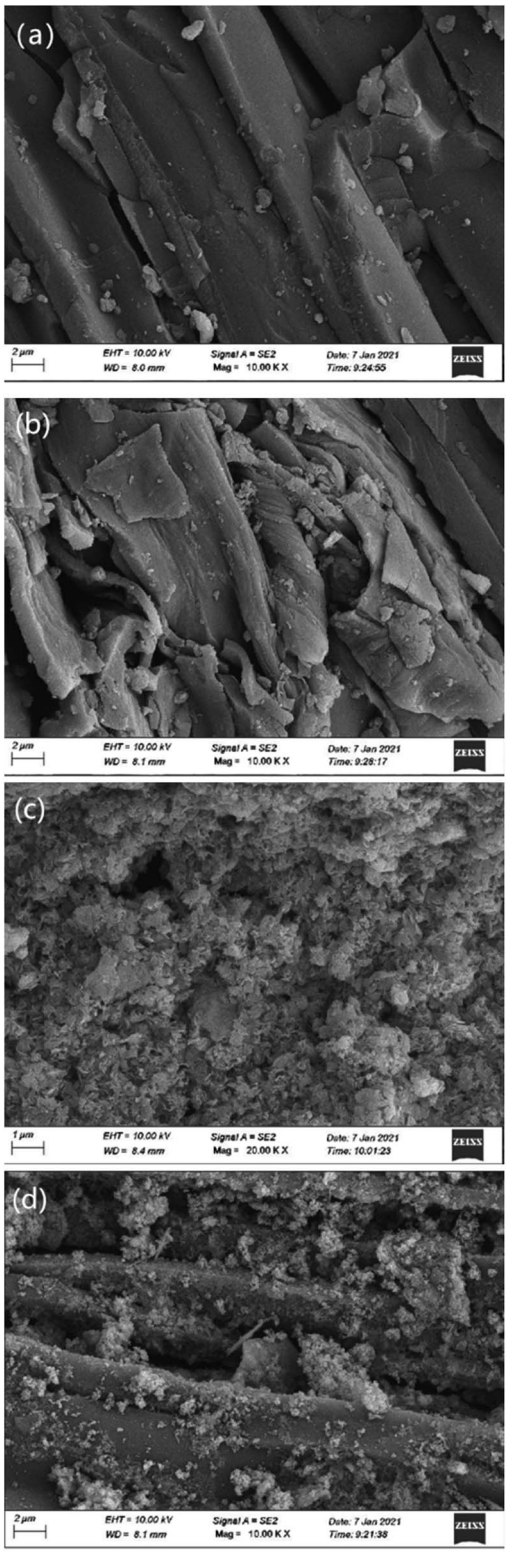


Fig. 3 SEM images of lignite and nFeS-lignite before and after reaction. (a) Lignite before reaction. (b) Lignite after reaction. (c) nFeS-lignite before reaction. (d) nFeS-lignite after reaction.

with $H^+$ to form $H_2S$ and separate from the reaction system in the form of gas. The rest $S^{2-}$ will form $Cr_2S_3$ precipitation with Cr(III). $Fe^{3+}$ generated after the reaction of $Fe^{2+}$ with Cr(VI) will

Table 3 Element content of lignite and nFeS-lignite before and after reaction

| | Element proportion/% | | | | |
|---|---|---|---|---|---|
| Type | C | O | S | Cr | Fe |
| Before lignite reaction | 75.85 | 20.23 | 2.58 | 0.00 | 1.34 |
| After lignite reaction | 73.12 | 20.57 | 3.41 | 1.01 | 1.89 |
| Before nFeS-lignite reaction | 28.58 | 15.96 | 17.80 | 0.00 | 37.66 |
| After nFeS-lignite reaction | 26.00 | 18.88 | 13.04 | 4.52 | 37.57 |

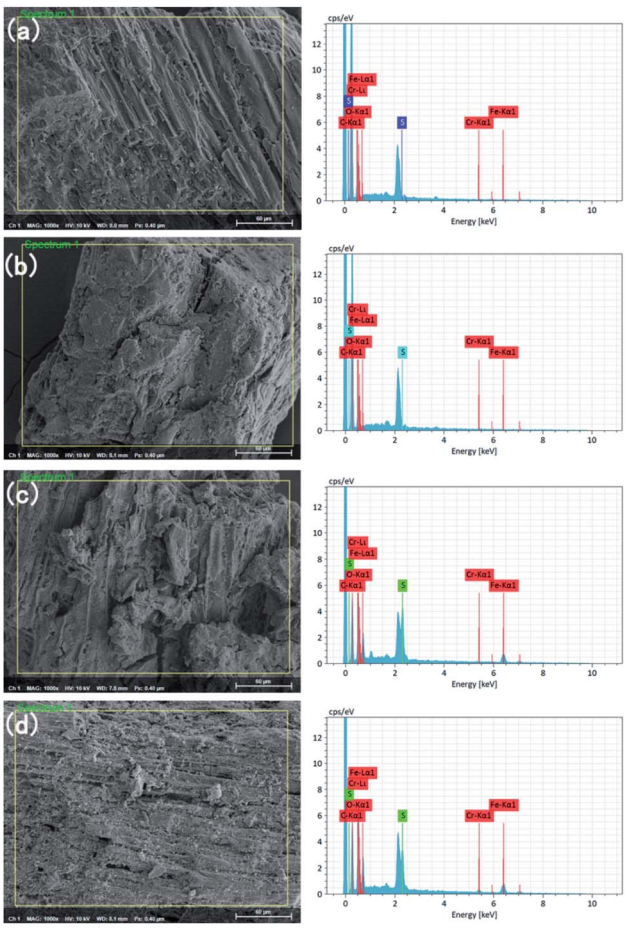


Fig. 4 EDS images of lignite and nFeS-lignite before and after reaction. (a) Lignite before reaction. (b) Lignite after reaction. (c) nFeS-lignite before reaction. (d) nFeS-lignite after reaction.

hydrolyze to form FeOOH precipitation, and these precipitates will re adhere to the surface of nFeS-lignite.

### 3.4 Fourier infrared spectroscopy

Fig. 5 is the Fourier transform infrared spectrum of lignite and nFeS-lignite before and after reaction.

Through the FTIR test of the material, according to the wave number attribution of the functional group absorption band, the infrared spectrum curve can be divided into four parts: aromatic hydrocarbon (900–700 $cm^{-1}$), oxygen-containing functional group (1800–1000 $cm^{-1}$), fatty hydrocarbon (3000–

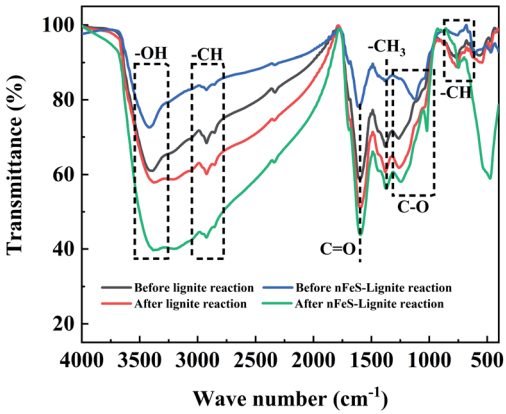


Fig. 5 FTIR images of lignite and nFeS-lignite before and after reaction.

28 000 $cm^{-1}$) and hydrogen bond (3600–3000 $cm^{-1}$).[21] In order to better understand the distribution of functional groups in the material, peak fitting of the infrared spectrum curve is carried out by using peakfit 4.12 software, so that the similarity $R^2$ between the fitting curve generated by superposition after peak splitting and the experimental curve is at least more than 0.95. The fitting diagram is shown in Fig. 6.

**3.4.1 Analysis of aromatic hydrocarbon absorption band.** As can be seen from Fig. 6a, in the aromatic hydrocarbon absorption band with wave number of 900–700 $cm^{-1}$, the absorption peak mainly comes from the aromatic substituted functional groups generated by the out of plane deformation and vibration of C–H bond on the benzene ring. It can be seen from the area percentage in Fig. 6a that benzene ring disubstitution is the main substitution mode of benzene ring in each sample. Compared with that before the reaction, the proportion of benzene ring disubstitution decreased from 72.16% to 61.41%, and the proportion of benzene ring tetrasubstitution increased from 10.58% to 24.62%; after lignite reaction, the proportion of benzene ring disubstitution decreased from 72.26% to 54.66%, and the proportion of benzene ring trisubstitution increased from 23.52% to 40.70%. It shows that the aliphatic side chain and other atoms on the benzene ring of the adsorbent are unstable and will be broken due to the substitution reaction in the reaction process, resulting in an increase in the proportion of substituted aromatics.

**3.4.2 Absorption band analysis of oxygen-containing functional groups.** As can be seen from Fig. 6b, in the oxygen-containing functional group absorption band with wave number of 1800–1000 $cm^{-1}$, the absorption peaks mainly come from hydroxyl, carboxyl, carbonyl, ether oxygen, as well as $-CH_3$, $-CH_2$ bending vibration and C=C stretching vibration. It can be seen from the area percentage in Fig. 6b that the proportion of reducing functional groups such as(C–O phenols, ethers and C–O in aryl ethers), $-CH_3$ and $-CH_2$ (symmetric Ar-$CH_3$ and asymmetric $-CH_3$, $-CH_2$) of nFeS-lignite and lignite decreased after the reaction, while the total proportion of C=C (aromatic C=C) and carboxyl (–COOH) increased, indicating that the

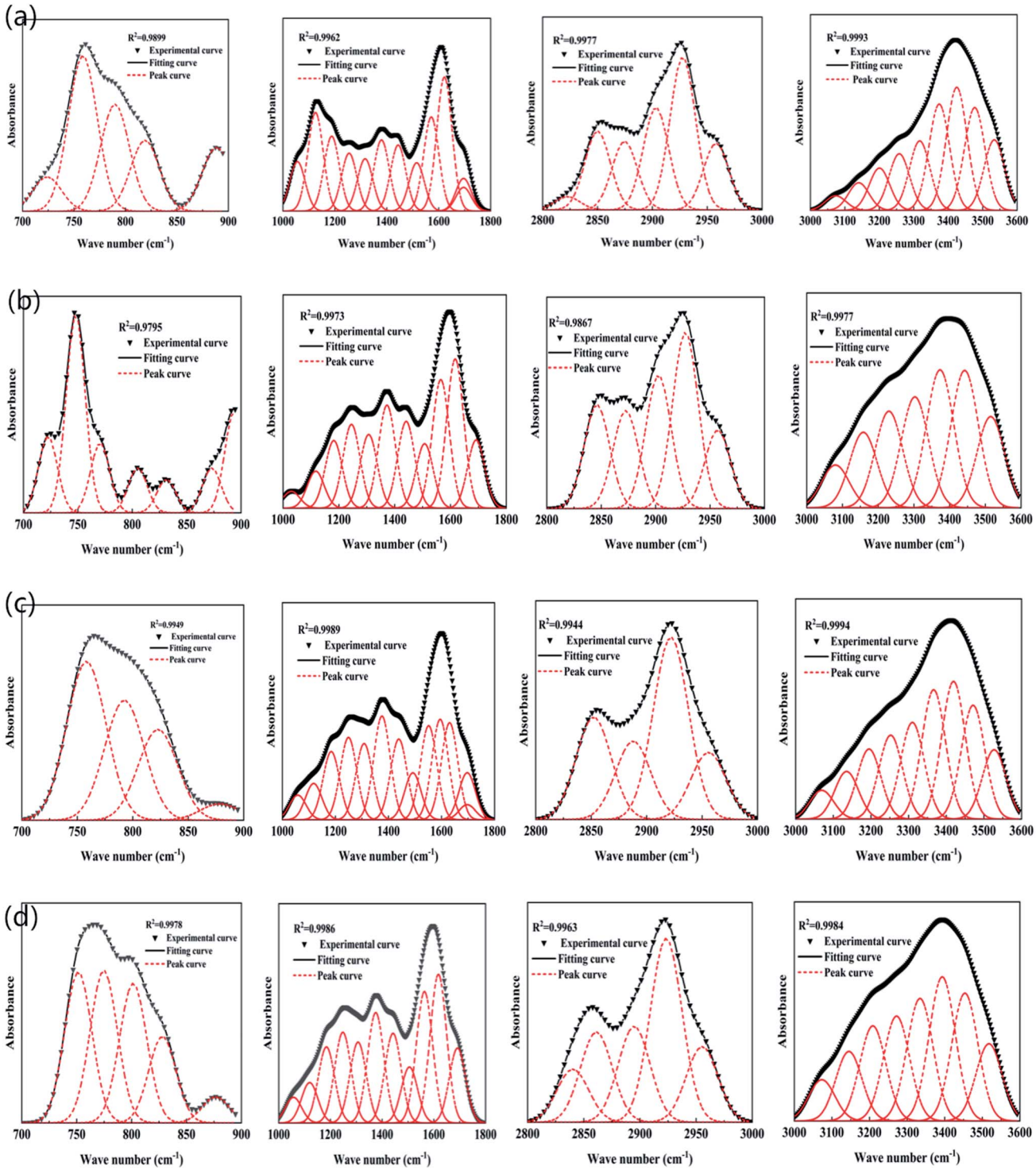


Fig. 6 Band peak fitting diagram of nFeS-lignite and lignite before and after reaction (a) nFeS-lignite before reaction band split peak fitting diagram. (b) nFeS-lignite after reaction band split peak fitting diagram. (c) Peak fitting diagram of lignite in the band before reaction. (d) Wave band split peak fitting diagram of lignite after reaction.

reducing groups of the adsorbent participated in the reduction of Cr(VI) to Cr(III). The reaction itself is oxidized to form functional groups such as C=C and C=O.[22]

**3.4.3 Analysis of fatty hydrocarbon absorption zone.** As can be seen from Fig. 6c, in the fatty hydrocarbon absorption zone with wave number of 3000–2800 $cm^{-1}$, the absorption peak mainly comes from the stretching vibration of C–H. It can be seen from the area percentage in Fig. 6c that after the reaction of nFeS-lignite and lignite, the proportion of –CH stretching vibration peak ($R_3CH$) decreases greatly, the proportion of $-CH_3$

antisymmetric stretching vibration peak (asymmetric $RCH_3$) fluctuates to a certain extent, and the total amount of $-CH_2$ stretching vibration peak (asymmetric $R_2CH_2$, symmetric $R_2CH_2$) increases, indicating that the lignite skeleton becomes loose during the reaction of nFeS-lignite and lignite, The structure of fat side chain was destroyed, so that the total amount of $-CH_3$ and $-CH_2$ did not decrease significantly after participating in redox reaction.[23]

**3.4.4 Hydroxyl absorption band analysis.** As can be seen from Fig. 6d, in the hydroxyl absorption band with wave number of 3600–3000 $cm^{-1}$, the absorption peak can be divided into four types according to the different hydrogen bond formation modes of hydroxyl: hydroxyl nitrogen hydrogen bond (OH–N), self associating hydroxyl hydrogen bond (phenol OH), ring hydrogen bond and hydroxyl–π hydrogen bond (OH–π).[24] It can be seen from the area percentage in Fig. 6d that the existing form of hydrogen bond in the samples before and after the reaction of nFeS-lignite and lignite is mainly self associating hydroxyl hydrogen bond. After the reaction, the proportion of self associating hydroxyl hydrogen bond decreases, and the proportion of cyclic hydrogen bond and hydroxyl–π hydrogen bond increases. This is because the content of oxygen-containing functional groups changes during the adsorbent reaction, the condensation degree of aromatic rings decreases, and the tightness of molecular internal spatial arrangement decreases, which greatly reduces the formation probability of self associating hydroxyl groups and enhances the hydroxyl–π bond.[25]

### 3.5 Analysis of Cr(VI) removal effect

The dynamic change of Cr(VI) removal percentage in the dynamic test of nFeS-lignite treatment of acid chromium containing wastewater is shown in Fig. 7.

According to the main functions and reaction modes of nFeS-lignite components in different periods, the change of Cr(VI) removal percentage of 1# column in 25 day column test cycle can be summarized into four stages. According to previous studies, the removal rate of Cr(VI) by FeS is fast, and the removal effect can reach more than 90%. So in the first stage of the reaction (0–4 days), the content of nano FeS loaded by nFeS-lignite is rich, which can quickly oxidize Cr(VI) in wastewater and achieve the effect of complete removal. In the second stage of the reaction (5–12 days), the Cr(VI) removal percentage decreased with the continuous consumption of nano FeS, and the decrease was more and more obvious. On the 12th day, the Cr(VI) removal percentage had decreased to 70.9%. Although lignite participated in the first two stages, the reaction was mainly nano FeS. The third stage of the reaction (13–19 days): the turning point in the removal rate of Cr(VI) indicates that nano FeS does not occupy a dominant position in the treatment of wastewater by nFeS-lignite. At this time, the reducing functional groups in lignite are mainly used to remove Cr(VI) from wastewater. The significant decrease in removal rate at the 17th to 19th day may be caused by the rapid decrease in the number of reducing functional groups in lignite. In the fourth stage of the reaction (20–25 days),

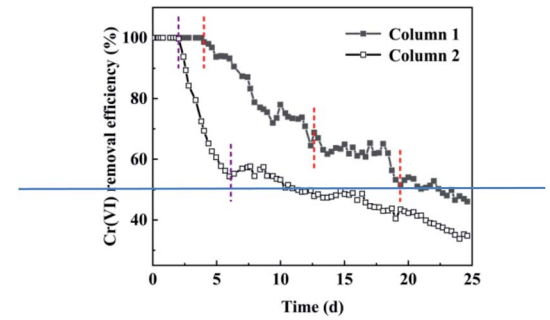


Fig. 7 The result of dynamic experiment on removal percentages of Cr(VI).

Table 4 The removal rate of Cr(VI) by adsorbent

| Adsorbent | Removal percentage (%) | References |
|---|---|---|
| nFeS-lignite | 71.6 | Present study |
| Lignite | 54.4 | Present study |
| Flyash | 23.33 | 26 |
| Calcined modified flyash | 57.75 | 26 |
| OTAC modified zeolite | 32.22 | 27 |
| AlZr pillared montmorillonite | 61 | 28 |
| Bentonite | 10.89 | 29 |
| Biological medical stone particles | 70.1 | 30 |

although the removal percentage of Cr(VI) fluctuated, the overall downward trend was not obvious. At the end of the test on the 25th day, it decreased to 46.1%. At this time, the removal of Cr(VI) mainly depended on the adsorption of Cr(VI) by the adsorption site of lignite itself. After 25 days of operation, the average removal percentage of Cr(VI) by 1# dynamic column was 71.6%.

The change of Cr(VI) removal percentage of 2# column is relatively simple, which can be summarized into three stages: the first stage of reaction (0–2 days), the second stage of reaction (3–7 days) and the third stage of reaction (8–25 days). Cr(VI) removal percentage changed gradually with the consumption of reducing functional groups of lignite in the first two stages, and decreased steadily with the decrease of adsorption sites after the reaction entered the eighth day. At the same time, the change trend of Cr(VI) removal percentage of 2# column in the third stage of reaction is similar to that of 1# column, which again confirms that lignite adsorption is the main removal mechanism of 1# column after 20 days of reaction. After 25 days of operation, the 2# dynamic column had an average removal percentage of Cr(VI) of 54.4% (Table 4).

### 3.6 Analysis of total chromium removal effect

The total chromium removal percentage in the dynamic test of nFeS-lignite for the treatment of acid chromium containing wastewater is shown in Fig. 8.

The change of total chromium removal percentage of 1# column in the 25 day column test cycle can also be summarized into four stages, but the time division is different: the

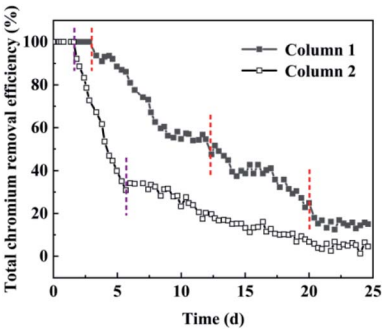


Fig. 8 The result of dynamic experiment on removal percentages of total chromium.

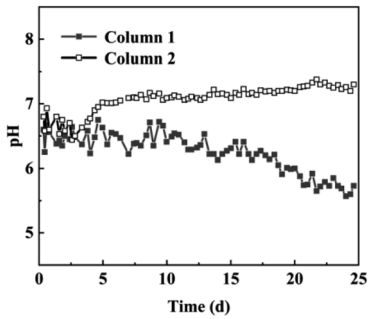


Fig. 9 The result of dynamic experiment on pH change.

first stage of reaction (0–3 days), the second stage of reaction (4–12 days), the third stage of reaction (13–20 days) and the fourth stage of reaction (21–25 days). The change of total chromium removal percentage of 2# column can be summarized into three stages: the first stage of reaction (0–2 days), the second stage of reaction (3–5 days) and the third stage of reaction (6–25 days). In the first two stages of 1# column reaction, $Fe^{2+}$ produced by nano FeS ionization reacts with Cr(VI) to form $Fe^{3+}$ and Cr(III), and $S^{2-}$ reacts with Cr(III) to form $Cr_2S_3$ precipitation. This process will cause the pH of the solution to rise. Therefore, $Fe^{3+}$ hydrolyzes to form FeOOH and $Fe(OH)_3$ precipitates, which play a certain role in adsorption and complexation of Cr(III). Cr(III) itself will also form $Cr(OH)_3$ precipitates, so that the 1# column can maintain a high total chromium removal percentage. With the consumption of nano FeS, the removal mechanism of total chromium by 1# column is gradually similar to that of 2# column. Both rely on the oxygen-containing functional groups on the lignite surface to form –O–Cr–O structure with Cr(III), so as to fix and remove Cr(III).[34,35] In the final reaction stage, 1# column and 2# column mainly dynamically remove chromium ions from wastewater through lignite adsorption sites. The total chromium removal percentage decreases steadily with the reduction of adsorption sites. At the end of the test on the 25th day, the total chromium removal percentages of the two dynamic columns are 15.1% and 4.56% respectively. At this time, the adsorption capacity of 2# column for chromium ions is close to the saturation value. After 25 days of operation, the average removal percentages of total chromium by 1# column and 2# column were 53.1% and 28.8% respectively (Table 5).

Table 5 The removal rate of total chromium by adsorbent

| Adsorbent | Removal percentage (%) | References |
|---|---|---|
| nFeS-lignite | 53.10 | Present study |
| Lignite | 28.80 | Present study |
| Sugarcane waste residue | 46.50 | 31 |
| HCl acid modified bamboo shell | 45.41 | 32 |
| Flyash | 34.00 | 33 |
| Biological medical stone particles | 65.92 | 30 |

### 3.7 pH change analysis

The pH change curve of the dynamic test of nFeS-lignite for the treatment of acid chromium containing wastewater is shown in Fig. 9.

It can be seen from Fig. 9 that 1# column and 2# column have good effect on improving the pH of wastewater. Comparing the Cr(VI) and total chromium removal percentage curves in Fig. 7 and 8, it can be seen that the pH change of 1# column during 0–12 days of reaction is mainly affected by nano FeS reaction. The ionization process of nano FeS needs to consume $H^+$, and the $S^{2-}$ produced by ionization can combine with $H^+$ to form $HS^-$ or $H_2S$, which is separated from the wastewater in the form of gas. Therefore, although the pH of the effluent of the 1# column fluctuates, it remains at about 6.6.[36] After the 13th day of the reaction, lignite in nFeS-lignite became the main force for chromium removal, so the pH of effluent gradually decreased to 5.3 at the end of the test on the 25th day, because the kaolinite and other mineral components of lignite were affected during the preparation of nFeS-lignite, and the ability of adsorbent to adjust pH was weakened. In the early stage of the reaction, the 2# column mainly relies on the active groups of lignite to remove chromium ions. These acidic organic matter can not effectively improve the pH of wastewater when reacting with chromium,[37] so that the pH of effluent from the 2# column fails to reach neutral during the reaction period of 0–5 days. With the continuous progress of the reaction, the alkaline mineral composition of lignite wrapped by organic matter gradually revealed, effectively neutralized the acidic wastewater, and the pH of 2# column effluent gradually increased to 7.3 at the end of the test on the 25th day.

## 4 Conclusion

(1) By constructing two groups of dynamic column experimental models of nFeS-lignite and lignite particles to treat acid chromium containing wastewater, the long-term treatment capacity of nFeS-lignite for acid chromium containing wastewater was explored. The test results show that after 25 days of operation of the dynamic column, 1# the average removal percentages of Cr(VI) and total chromium by the dynamic column are 71.6% and 53.1% respectively, the effluent pH is reduced from 6.6 to 5.3, 2# the average removal percentages of Cr(VI) and total chromium by the dynamic column are 54.4% and 28.8%

respectively, and the effluent pH is increased from 6.6 to 7.3, indicating that the nano FeS loaded nFeS-lignite has a better remediation effect on acid chromium containing wastewater.

(2) SEM, EDS and FTIR analysis showed that after the reaction of nFeS-lignite and lignite, the structure was eroded, the surface folds increased and a large number of sediment crystals appeared. Reducing groups such as $-CH_3$, $-CH_2$, C–O and Ar-OH participated in the reaction and were oxidized to C=O, C=O and other groups. New diffraction peaks such as FeOOH, $Cr(OH)_3$ and $Cr_2S_3$ appeared in the XRD spectrum after nFeS-lignite reaction, indicating that after Cr(VI) was reduced to Cr(III), it would be fixed on the surface of nFeS-lignite in the form of precipitation such as hydroxide and sulfide.

## Author contributions

Conceptualization: Xuying Guo and Saiou Fu; methodology, Xuying Guo; software, Xuying Guo and Xinle Gao; validation, Xuying Guo, and Yanrong Dong; formal analysis, Xuying Guo; investigation, Xuying Guo and Guoliang Jiang; resources, Xinle Gao and Zhiyong Hu; data curation, Xuying Guo and Xinle Gao; writing—original draft preparation, Xinle Gao; writing—review and editing, Guoliang Jiang and Yanrong Dong; visualization, Xuying Guo; supervision, Yanrong Dong and Saiou Fu; project administration, Guoliang Jiang and Saiou Fu; all authors have read and agreed to the published version of the manuscript.

## Conflicts of interest

There are no conflicts to declare.

## Acknowledgements

The project is funded by the National Natural Science Foundation of China (51304114), Department of Education of Liaoning Province (LJ2017FAL016, LJKZ0340).

## References

1 C. Wang, Y. Jiang, J. Shang, B. Zhu and Y. Chen, *Liaoning Chem. Ind.*, 2021, **50**(6), 828–830.
2 B. Saha and C. Orvig, *Coord. Chem. Rev.*, 2010, **254**(23), 2959–2972.
3 S. Zink, R. Schoenberg and M. Staubwasser, *Geochim. Cosmochim. Acta*, 2010, **74**, 5729–5745.
4 N. Kocberber and G. Donmez, *Bioresour. Technol.*, 2007, **98**(11), 2179–2183.
5 N. Unceta, F. Séby, J. Malherbe and O. F. X. Donard, *Anal. Bioanal. Chem.*, 2010, **397**(3), 1097–1111.
6 P. Venkateswaran and K. Palanivelu, *Hydrometallurgy*, 2005, **78**(12), 107–115.
7 J. L. P. Sheeja, *Orient. J. Chem.*, 2016, **32**(4), 2209–2213.
8 G. Kaur, S. J. Couperthwaite, B. W. Hatton-Jones and G. J. Millar, *J. Water Process. Eng.*, 2018, **22**, 46–58.
9 M. Pratima, A. Ghosh, Y. Ramamurthy, B. D. Pandey and M. L. Torem, *Russian Journal of Non-Ferrous Metals*, 2018, **59**(5), 533–542.
10 B. Dinaol, A. Kenatu, T. Amare, K. Helmut and F. Jemal, *Energy Ecol. Environ.*, 2020, **5**(3), 184–195.
11 F. Li, R. Li and J. Wen, *Chemical Engineer*, 2022, **36**(1), 47–49.
12 M. A. Nazir, M. A. Bashir, T. Najam, M. S. Javed, S. Suleman, S. Hussain, O. P. Kumar, S. S. A. Shah and A. Rehman, *Microchem. J.*, 2021, **164**(8), 105973.
13 M. A. Nazir, N. A. Khan, C. Cheng, S. S. A. Shah and A. U. Rehman, *Appl. Clay Sci.*, 2020, **190**, 105564.
14 N. A. Khan, S. Shaheen, T. Najam, S. S. A. Shah, M. S. Javed, M. A. Nazir, E. Hussain, A. Shaheen, S. Hussain and M. Ashfaq, *Toxin Rev.*, 2020, **2020**, 1–13.
15 Y. Liu, W. Xiao, J. Wang, A. M. Zakaria, W. Tao and M. Jae-Min, *J. Nanomater.*, 2016, **2016**, 1–9.
16 Y. Yang, Y. Xie and X. Li, *J. Environ. Biol.*, 2015, **36**(2), 393–398.
17 Q. Zhao, *Clean Coal Technol.*, 2018, **24**(2), 9–14.
18 S. Jellali, A. A. Azzaz, M. Jeguirim, H. Hamdi and A. Mlayah, *Water*, 2021, **13**(2), 164.
19 J. Di, J. Liu, J. Guo and S. Fu, *Journal of Water Resources and Water Engineering*, 2020, **31**(1), 29–32.
20 X. Guo, S. Fu, J. Di and Y. Dong, *Coal Sci. Technol.*, 2020, **48**(9), 152–159.
21 H. Xin, D. Wang, X. Qi, G. Qi and G. Dou, *Fuel Process. Technol.*, 2014, **118**, 287–295.
22 T. Zhao, W. Ge, F. Yue, Y. Wang, C. M. Pedersen, F. Zeng and Y. Qiao, *Fuel Process. Technol.*, 2016, **152**, 375–380.
23 C. Liang, W. Liang and W. Li, *Coal Sci. Technol.*, 2020, **48**(S1), 182–186.
24 C. Li, J. Wang, L. Dong, Y. Sun and X. Cao, *Spectrosc. Spectral Anal.*, 2014, **34**(11), 2961–2967.
25 P. Hao, Y. Meng, F. Zeng, T. Yan and G. Xu, *Spectrosc. Spectral Anal.*, 2020, **40**(3), 787–792.
26 J. Cheng, M. Huang and S. Cai, *Complex Utilization of Valuable Minerals*, 2022, **2022**, 1–8.
27 X. Wu, W. Chen, H. Zhang, H. Zheng, Y. Lu and R. Zhang, *Industrial Safety and Environmental Protection*, 2018, **44**(11), 67–71.
28 G. Weng, X. Li, D. Yang and Y. Li, *J. Fuzhou Univ.*, 2003, **2003**(1), 116–119.
29 J. Zhang, S. Li, Q. Wu, A. Wei, P. Ning and D. Zhang, *Guangzhou Chem.*, 2016, **41**(6), 46–49.
30 J. Di, H. Xu, W. Zhao, G. Jiang, J. Guo, J. Liu and X. Lin, *Ind. Water Treat.*, 2019, **39**(12), 33–36.
31 R. Wang and H. Xu, *Water Treat. Technol.*, 2017, **43**(11), 77–79.
32 H. Fang, *Chem. Eng., Equip.*, 2012, **2012**(6), 191–196.
33 X. Pan, S. Wang, W. Tong and A. Chang, *Environmental Pollution Control Technology and Equipment*, 2003, **2003**(12), 36–39.
34 J. Di, X. Lin and Y. Dong, *Non-Met. Mines*, 2019, **42**(6), 86–89.
35 L. Kang, H. Yang, L. Wang, S. Chai, R. Zhang, J. Wu and X. Liu, *J. Hazard. Mater.*, 2020, **398**, 122834.
36 H. Tian, J. Li, Z. Mu, L. Li and Z. Hao, *Sep. Purif. Technol.*, 2009, **66**(1), 84–89.
37 X. Gu, *Humic Acid*, 2021, (1), 24–28.